



On accuracy of the finite-difference and finite-element schemes with respect to P -wave to S -wave speed ratio

Peter Moczo,¹ Jozef Kristek,¹ Martin Galis¹ and Peter Pazak²

¹*Faculty of Mathematics, Physics and Informatics, Comenius University Bratislava, Mlynska dolina F1, 842 48 Bratislava, Slovak Republic.*

E-mail: moczo@fmph.uniba.sk

²*Geophysical Institute, Slovak Academy of Sciences, Dubravska cesta 9, 845 28 Bratislava, Slovak Republic*

Accepted 2010 April 21. Received 2010 April 16; in original form 2009 September 21

SUMMARY

Numerical modelling of seismic motion in sedimentary basins often has to account for P -wave to S -wave speed ratios as large as five and even larger, mainly in sediments below groundwater level. Therefore, we analyse seven schemes for their behaviour with a varying P -wave to S -wave speed ratio. Four finite-difference (FD) schemes include (1) displacement conventional-grid, (2) displacement-stress partly-staggered-grid, (3) displacement-stress staggered-grid and (4) velocity–stress staggered-grid schemes. Three displacement finite-element schemes differ in integration: (1) Lobatto four-point, (2) Gauss four-point and (3) Gauss one-point. To compare schemes at the most fundamental level, and identify basic aspects responsible for their behaviours with the varying speed ratio, we analyse 2-D second-order schemes assuming an elastic homogeneous isotropic medium and a uniform grid. We compare structures of the schemes and applied FD approximations. We define (full) local errors in amplitude and polarization in one time step, and normalize them for a unit time. We present results of extensive numerical calculations for wide ranges of values of the speed ratio and a spatial sampling ratio, and the entire range of directions of propagation with respect to the spatial grid.

The application of some schemes to real sedimentary basins in general requires considerably finer spatial sampling than usually applied.

Consistency in approximating first spatial derivatives appears to be the key factor for the behaviour of a scheme with respect to the P -wave to S -wave speed ratio.

Key words: Numerical approximations and analysis; Computational seismology; Theoretical seismology.

1 INTRODUCTION

The structural complexity of realistic models in theoretical modelling of seismic wave propagation and earthquake ground motion makes it impossible to apply exact (analytical) methods. Approximate computational methods have to be used. Accuracy and computational efficiency of a method are often contradictory. It is just the reasonable and optional balance between the accuracy and computational efficiency in case of complex realistic structures, which made the numerical modelling methods dominant among all approximate methods.

Different numerical modelling methods have been developed in the last few decades—for example, finite-difference method (FDM), finite-element method (FEM), spectral-element method (SEM), arbitrary-high-derivative—discontinuous Galerkin method (ADER-DGM). FDM and FEM have relatively long traditions. SEM has been used since the early 1990s of the last century (e.g. Seriani & Priolo 1991, 1994; Komatitsch & Vilotte 1998; Komatitsch & Tromp, 1999; Komatitsch *et al.* 2001; for a comprehensive review see Chaljub *et al.* 2007). ADER-DGM has been elaborated and applied to seismology rather recently (Dumbser & Käser 2006; Käser & Dumbser 2006; Dumbser *et al.* 2007; Käser *et al.* 2007; de la Puente *et al.* 2007, 2008; Käser *et al.* 2008).

Despite the relatively long tradition of FDM and FEM, they are still being developed in terms of accuracy and efficiency, and it is reasonable to expect considerable improvements in the future. Despite the existence and development of more sophisticated methods, mainly SEM and ADER-DGM, the FDM is still widely applied to a variety of problems in the earthquake and exploration seismology. In this study, we primarily focus on FDM, but we also include FEM for comparison.

In the early days of application of FDM, the displacement (D) formulation of the equation of motion and conventional grids (all displacement components at each gridpoint) were used (e.g. Alterman & Karal 1968; Alterman & Rotenberg 1969; Alterman & Loewenthal 1970; Boore 1970, 1972; Alford *et al.* 1974; Ilan *et al.* 1975; Kelly *et al.* 1976; for a review of more recent elaborations see Moczo

et al. 2007a). Bamberger *et al.* (1980) analysed grid dispersion and found that the ratio of the numerical *S*-wave phase velocity to the true *S*-wave velocity becomes infinite inside liquids for conventional FD schemes. Stephen (1983), based on numerical tests, pointed out instabilities of the heterogeneous conventional FD schemes at a liquid/solid interface. Marfurt (1984) analysed grid dispersion and concluded that in a homogeneous elastic medium the explicit FE and FD schemes are comparable for Poisson's ratio less than 0.3; FE scheme is superior to FD for Poisson's ratio between 0.3 and 0.45 and none of the schemes is economically attractive for Poisson's ratio greater than 0.45.

Problems with instabilities and inaccuracy of the conventional FD schemes led Virieux (1984, 1986) to introduce the staggered-grid (each particle-velocity and stress-tensor component has its own grid position except that the normal stress-tensor components share the same position) velocity–stress (VS) FD schemes for modelling seismic wave propagation. Virieux (1986) found that the stability condition of his *P*–*SV* VS staggered-grid scheme as well as the numerical *P*-wave phase velocity is independent of Poisson's ratio. The numerical *S*-wave phase velocity depends on the Poisson's ratio but is rather insensitive to the Poisson's ratio, and its behaviour does not degrade as the Poisson's ratio goes to 0.5. None of these properties is the case for the conventional FD schemes.

The staggered-grid FD schemes have become the dominant type of schemes in the FD modelling of seismic wave propagation and earthquake motion. Levander (1988) applied the fourth-order approximation in space to the *P*–*SV* scheme. Luo & Schuster (1990) introduced the *P*–*SV* displacement–stress (DS) scheme. The application of the fourth-order 3-D staggered-grid schemes was considerably promoted by Olsen *et al.* (1995), Graves (1996) and Pitarka (1999). Moczo *et al.* (2002) presented a fourth-order staggered-grid scheme based on a heterogeneous formulation of the equation of motion, and numerically demonstrated superior accuracy of their scheme in heterogeneous media compared to the previous staggered-grid schemes. The improvement was achieved by the effective material grid parameters based on an analysis of consistency of the scheme with boundary conditions on a material interface.

As Virieux (1986) did for his second-order scheme, Levander (1988) analysed grid dispersion of his fourth-order *P*–*SV* scheme. Crase *et al.* (1992) derived stability condition for the *P*–*SV* case of an arbitrary order of approximation using a decomposition of the matrix scheme and a Fourier transform. Rodrigues & Mora (1992) analysed grid dispersion in the 3-D case. Igel *et al.* (1995) extended the analyses in the two latter studies for a general 3-D elastic anisotropic case. Klimeš (1996) investigated the error in the phase velocity in several 2-D and 3-D conventional and staggered-grid schemes. He found that the staggered-grid schemes are more efficient than the conventional schemes with the same accuracy if the *P*-wave to *S*-wave speed ratio is smaller than $\sqrt{3}$, and with a much better accuracy if the speed ratio is considerably larger than $\sqrt{3}$. Moczo *et al.* (2000a,b) presented a derivation of the stability condition and grid dispersion in the 2-D/3-D fourth-order in space, second-order in time, DS FD schemes and numerical investigation of the grid dispersion in space, coordinate-axis plane, body-diagonal plane and three distinct directions of propagation for different values of the Poisson's ratio.

The staggered-grid FD schemes enabled seismologists to model seismic wave propagation and earthquake ground motion in heterogeneous viscoelastic isotropic models that were practically impossible for the conventional FD schemes. However, the need to model seismic wave propagation in anisotropic media soon confronted the staggered-grid schemes with their inherent limitation—staggered distribution of the particle-velocity and stress-tensor components in the grid.

In the partly-staggered grid, all particle-velocity components are located at the same grid position, and all stress-tensor components are located at another grid position. Thus, no interpolation of particle velocities or strains is necessary. This was the reason why Magnier *et al.* (1994) used the partly-staggered grid to incorporate anisotropy. Note, however, that the partly-staggered grid was applied earlier by Andrews (1973) and independently by Day (1977, 1982) in their modelling of the fault rupture propagation. Later Zhang (1997) applied the partly-staggered grid, and recently the schemes based on this type of grid have been promoted by Saenger and his colleagues (e.g. Saenger *et al.* 2000; Saenger & Bohlen 2004).

Saenger *et al.* (2000) report that dispersion relations for their scheme are independent of the Poisson's ratio and that this property allows handling the liquid–solid contact without applying boundary conditions. The schemes on the partly-staggered grids suffer from the presence of the hour-glass modes. The modes have to be artificially suppressed.

Although the partly-staggered spatial distribution of the field variables is better than the (fully) staggered distribution for wave propagation modelling in anisotropic media and dynamic rupture modelling, it is still obvious that having all field variables at each grid position would be much better for a proper simulation of boundary conditions at material interfaces and faults.

The limitations of the staggered-grid and partly-staggered-grid schemes probably motivated Geller & Takeuchi (1995, 1998) and Takeuchi & Geller (2000) to develop their optimally accurate FD schemes on the conventional grid. The idea of Geller and Takeuchi was to minimize the error of the numerical solution first of all at eigenfrequencies, that is, at frequencies at which oscillatory motion of a linear mechanical system or finite volume of elastic continuum is naturally most amplified. They derived a general criterion that can be used to derive optimally accurate operators without knowing the actual values of the eigenfrequencies and eigenfunctions. Geller & Takeuchi (1995) showed that in the case of a heterogeneous medium the criterion is the logical extension of the criterion to minimize grid dispersion of phase velocity in a homogeneous medium. To our knowledge, however, Geller and Takeuchi did not show the behaviour of their scheme with the varying *P*-wave to *S*-wave speed ratio.

For more details on the historical development of the different types of FD schemes and their properties as well as for references, see, for example, reviews by Moczo *et al.* (2007a,b).

We just briefly mention that the application of FEM to seismology was pioneered by Lysmer (1970), Lysmer & Drake (1971, 1972) and Smith (1975). Recently, the application of FEM has been elaborated, for example, by Bielak *et al.* (2003), Yoshimura *et al.* (2003) and Ma & Liu (2006).

Kristek & Moczo (2006) presented a 1-D FD scheme that is based on the application of Geller & Takeuchi's (1998) optimally accurate FD operators to the heterogeneous strong-form equation of motion developed by Moczo *et al.* (2002). They numerically compared the scheme with two other FD schemes that approximate the heterogeneous strong-form equation of motion—one using conventional second-order FD operators, the other using staggered-grid fourth-order FD operators. Moczo *et al.* (2007a) developed a 3-D optimally accurate (satisfying the criterion by Geller & Takeuchi 1995) scheme with symmetric operators. Numerical tests of the scheme indicated insufficient accuracy in media with large P -wave to S -wave speed ratio. The unexpected problem led us to investigate the accuracy of FD schemes with respect to the varying P -wave to S -wave speed ratio.

Let us point out that numerical modelling of earthquake ground motion in sedimentary basins and valleys often has to account for the P -wave to S -wave speed ratios as large as five and even larger, mainly in sediments below groundwater level. The ratio can attain values larger than 10—unconsolidated lake sediments in Ciudad de México are a good example. At the same time, properties of FD schemes (and not only the FD schemes, in fact) with respect to the varying P -wave to S -wave speed ratio have not been sufficiently and consistently analysed yet.

In this study, we focus on the accuracy of FD and FE schemes with respect to the P -wave to S -wave speed ratio (say, r). We aim to identify and select the very basic inherent aspects of the schemes responsible for their behaviour with varying r and to compare different schemes at the most fundamental level. Therefore, we have to analyse the basic second-order 2-D numerical schemes on a uniform grid in a homogeneous medium. The second-order can be (practically) considered as the basic order of approximation, and the effect of r (or the Poisson's ratio) does not exist in a 1-D elastodynamic problem. We investigate four FD and three FE schemes.

- (1) FD displacement on a conventional grid (FD_D_CG),
- (2) FD displacement-stress on a partly-staggered grid (FD_DS_PSG),
- (3) FD displacement-stress on a staggered grid (FD_DS_SG),
- (4) FD velocity-stress on a staggered grid (FD_VS_SG),
- (5) FE with Lobatto four-point integration (FE_L),
- (6) FE with Gauss four-point integration (FE_G) and
- (7) FE with Gauss one-point integration (FE_G1).

Unlike previous analyses of accuracy, we do not investigate the grid dispersion. Instead, we define and calculate (full) local errors of the schemes in amplitude and polarization in one time integration step. Because different schemes use different time steps (according to appropriate stability conditions), we normalize errors for a unit time. The normalization allows a direct comparison of errors of different schemes. We perform extensive numerical calculations for wide ranges of values of r and spatial sampling ratio, and for the entire range of directions of propagation with respect to the spatial grid.

In parallel with the analysis of the numerical results, we compare the numerical schemes themselves in terms of their inherent structures and applied FD approximations.

Although and, at the same time, because the schemes are the simplest possible, we find the differences between the schemes very interesting and somehow surprising.

2 EQUATIONS OF MOTION

Consider a Cartesian coordinate system (x, z) and a homogeneous perfectly elastic isotropic medium. Let ρ denote density, and λ and μ , Lamé elastic moduli. Let displacement components u_x, u_z , particle-velocity components v_x, v_z and stress-tensor components $\sigma_{xx}, \sigma_{zz}, \sigma_{xz}$ be functions of the spatial coordinates x, z and time t . Let

$$\varphi_{,\zeta} = \frac{\partial \varphi}{\partial \zeta}; \quad \varphi \in \{u_x, u_z, v_x, v_z, \sigma_{xx}, \sigma_{zz}, \sigma_{xz}\}, \quad \zeta \in \{t, x, z\}. \quad (1)$$

The DS formulation of the equations of motion is then

$$\begin{aligned} \rho u_{x,tt} &= \sigma_{xx,x} + \sigma_{xz,z} \\ \rho u_{z,tt} &= \sigma_{zz,z} + \sigma_{xz,x} \\ \sigma_{xx} &= (\lambda + 2\mu) u_{x,x} + \lambda u_{z,z} \\ \sigma_{zz} &= (\lambda + 2\mu) u_{z,z} + \lambda u_{x,x} \\ \sigma_{xz} &= \mu u_{x,z} + \mu u_{z,x} \end{aligned} \quad (2)$$

The D formulation is obtained by substituting the stress-tensor components in the two first equations.

$$\begin{aligned} \rho u_{x,tt} &= (\lambda + 2\mu) u_{x,xx} + \mu u_{x,zz} + (\lambda + \mu) u_{z,xz} \\ \rho u_{z,tt} &= (\lambda + 2\mu) u_{z,zz} + \mu u_{z,xx} + (\lambda + \mu) u_{x,xz} \end{aligned} \quad (3)$$

The VS formulation is an alternative to the DS formulation:

$$\begin{aligned}
 \rho v_{x,t} &= \sigma_{xx,x} + \sigma_{xz,z}, \\
 \rho v_{z,t} &= \sigma_{zz,z} + \sigma_{zx,x}, \\
 \sigma_{xx,t} &= (\lambda + 2\mu) v_{x,x} + \lambda v_{z,z}, \\
 \sigma_{zz,t} &= (\lambda + 2\mu) v_{z,z} + \lambda v_{x,x}, \\
 \sigma_{xz,t} &= \mu v_{x,z} + \mu v_{z,x}.
 \end{aligned}
 \tag{4}$$

Whereas the FDM is usually applied to one of the above strong forms of the equations of motion, the FEM (e.g. Zienkiewicz & Taylor 1989; Hughes 2000; Moczo *et al.* 2007a) solves the weak form of the equation of motion. Consider volume Ω of a medium with boundary Γ and prescribed traction (h_x, h_z) on part of boundary Γ , say Γ_N . Then the weak form of the equation of motion is

$$\begin{aligned}
 \int_{\Omega} w(\rho u_{x,tt}) d\Omega + \int_{\Omega} (w_{,x} \sigma_{xx} + w_{,z} \sigma_{xz}) d\Omega - \int_{\Gamma_N} w h_x d\Gamma &= 0, \\
 \int_{\Omega} w(\rho u_{z,tt}) d\Omega + \int_{\Omega} (w_{,x} \sigma_{zx} + w_{,z} \sigma_{zz}) d\Omega - \int_{\Gamma_N} w h_z d\Gamma &= 0.
 \end{aligned}
 \tag{5}$$

Eqs (5) have to be satisfied for all possible choices of weight functions w .

The P -wave and S -wave speeds are

$$\alpha = [(\lambda + 2\mu) / \rho]^{1/2} \quad \text{and} \quad \beta = (\mu / \rho)^{1/2},
 \tag{6}$$

and we denote the ratio of the speeds by r and Poisson's ratio by ν ,

$$r = \alpha / \beta, \quad \nu = (r^2 - 2) / 2(r^2 - 1).
 \tag{7}$$

3 NUMERICAL SCHEMES

We can solve systems of eqs (2)–(5) for an unbounded medium using a variety of numerical schemes. As we already pointed out in the Introduction, we want to analyse and compare the essential inherent features and differences between the numerical schemes in their behaviour with respect to the P -wave to S -wave speed ratio. Therefore, we have to analyse the most basic formulations in terms of the order of approximation (second-order) and dimensionality (2-D). We will investigate seven different basic and most common numerical schemes on a uniform grid and for a homogeneous medium.

We will consider FD and FE schemes constructed on three different spatial grids—conventional, partly-staggered and staggered. The three grids are depicted in Fig. 1. The grids are uniform with a grid spacing h in both directions. Time is discretized uniformly with Δt being a time step. $U_x^m(I, L)$ and $U_z^m(I, L)$ are discrete approximations to $u_x(Ih, Lh, m\Delta t) = u_x(x_I, z_L, t_m)$ and $u_z(Ih, Lh, m\Delta t) = u_z(x_I, z_L, t_m)$. Analogously, V_x, V_z, S_{xx}, S_{zz} and S_{xz} are discrete approximations to $v_x, v_z, \sigma_{xx}, \sigma_{zz}$ and σ_{xz} .

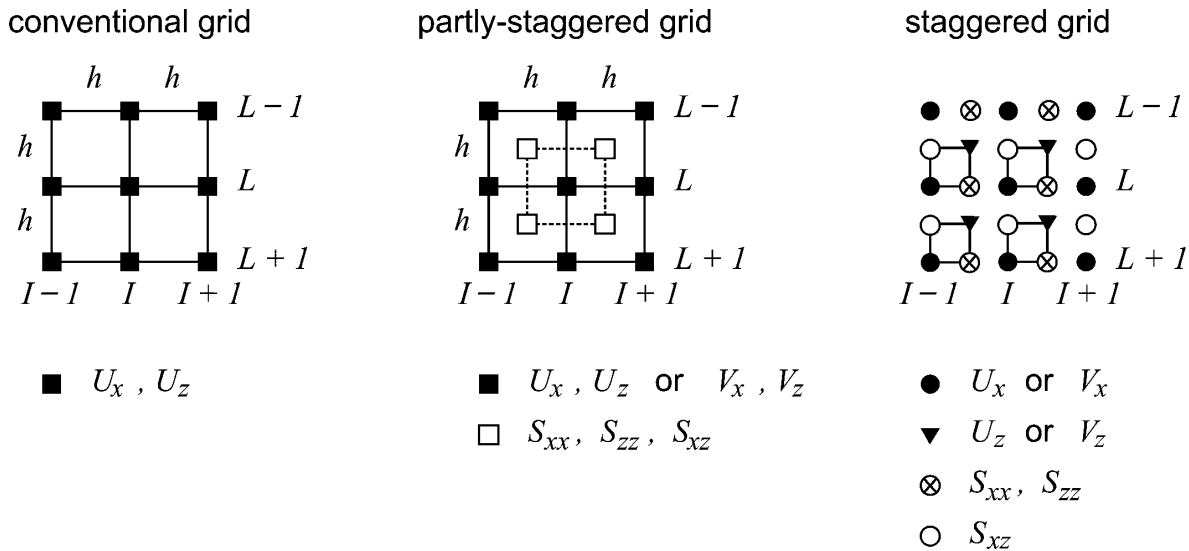


Figure 1. Three types of the spatial grids considered in this study. Left-hand side: conventional grid—both displacement components, U_x and U_z , are located at each gridpoint (position). Centre: partly-staggered grid—both displacement components U_x and U_z or particle-velocity components V_x and V_z share the same gridpoints, whereas all stress-tensor components, S_{xx}, S_{zz} and S_{xz} share other gridpoints. Right-hand side: staggered grid—each of the quantities has its own grid position except S_{xx} and S_{zz} sharing one grid position.

3.1 Scheme solving strong-form equations of motion for displacement on the conventional grid—FD_D_CG

A displacement conventional FD scheme for solving eqs (3) is obtained if derivatives in eqs (3) are replaced by standard second-order centred FD formulae (8) and (9) approximating second non-mixed and mixed derivatives. We denote the scheme as FD_D_CG. The scheme for the x -component, eq. (15), is shown together with all other schemes for a more convenient visual comparison of the schemes.

$$[\partial_{tt}\Phi]^m = \frac{1}{(\Delta t)^2} [\Phi^{m+1} - 2\Phi^m + \Phi^{m-1}], \quad (8)$$

$$[\partial_{xx}\Phi](I, L) = \frac{1}{h^2} [\Phi(I+1, L) - 2\Phi(I, L) + \Phi(I-1, L)],$$

$$[\partial_{zz}\Phi](I, L) = \frac{1}{h^2} [\Phi(I, L+1) - 2\Phi(I, L) + \Phi(I, L-1)],$$

$$[\partial_{xz}\Phi](I, L) = \frac{1}{4h^2} [\Phi(I+1, L+1) - \Phi(I+1, L-1) - \Phi(I-1, L+1) + \Phi(I-1, L-1)]. \quad (9)$$

3.2 Schemes solving weak-form equations of motion for displacement on the conventional grid—FE_L, FE_G and FE_G1

Consider quadrilateral elements with four nodes in vertices and with bilinear shape functions. In the case of a uniform grid (mesh), the elements become squares. In an application of the FE method to eqs (5) on the uniform grid we can use analytic or numerical integration. We considered three different integrations: standard Gauss four-point integration, reduced Lobatto four-point integration and reduced Gauss one-point integration. The Gauss four-point integration is exact in the case of the uniform grid and homogeneous medium. It leads to a computational scheme, say FE_G, eq. (16). The use of the Lobatto four-point integration (reduced integration, see, e.g. Zienkiewicz & Taylor 1989; Hughes 2000) leads to a computational scheme, say FE_L, which is exactly the same as FD_D_CG, that is, eq. (15). (We recall that we assume a homogeneous medium and uniform spatial grid.) Finally, the Gauss one-point integration is the simplest possible reduced integration. The corresponding scheme, say FE_G1, is given by eq. (17). Let us note that we use the term ‘conventional grid’ also for these three schemes to account for the fact that both displacement components are at all gridpoints (i.e. FE nodes), and stress-tensor components are not explicitly treated.

3.3 Scheme solving strong-form displacement-stress equations of motion on the partly-staggered grid—FD_DS_PSG

The equations in the DS formulation, eqs (2), can be solved by the DS FD scheme on the partly-staggered grid. First, we replace the second time derivatives using formula (8), and the first spatial derivatives of the stress-tensor components using formulae (10). We obtain a FD scheme for updating the displacement components. Then, we replace all discrete stress-tensor components on the right-hand side (r.h.s.) of the obtained scheme by their FD approximations. The approximations are obtained from the third to fifth equations of system (2) using formulae (10).

$$[\partial_x\Phi](I, L) = \frac{1}{2h} [\Phi(I+1/2, L-1/2) + \Phi(I+1/2, L+1/2) - \Phi(I-1/2, L-1/2) - \Phi(I-1/2, L+1/2)],$$

$$[\partial_z\Phi](I, L) = \frac{1}{2h} [\Phi(I-1/2, L+1/2) + \Phi(I+1/2, L+1/2) - \Phi(I-1/2, L-1/2) - \Phi(I+1/2, L-1/2)]. \quad (10)$$

This results in the FD scheme in which only displacement components appear. This fact is due to the DS formulation—eqs (2) do not include time derivatives of the stress-tensor components. We will call the scheme FD_DS_PSG. The scheme for the x -component is given by eq. (17). Note that the scheme is identical with the FE_G1.

3.4 Scheme solving strong-form displacement-stress equations of motion on the staggered grid—FD_DS_SG

The equations in the DS formulation, eqs (2), can also be solved by the DS FD scheme on the staggered grid. First, we replace the second time derivatives using formula (8), and the first spatial derivatives of the stress-tensor components using formulae (11),

$$[\partial_x\Phi](I, L) = \frac{1}{h} [\Phi(I+1/2, L) - \Phi(I-1/2, L)],$$

$$[\partial_z\Phi](I, L) = \frac{1}{h} [\Phi(I, L+1/2) - \Phi(I, L-1/2)]. \quad (11)$$

Then, we replace all discrete stress-tensor components on the r.h.s. of the obtained scheme by their FD approximations. The approximations are obtained from the third to fifth equations of system (2) using formulae (11). This results in the FD scheme in which only displacement

components appear. As in the case of the FD_DS_PSG scheme, this fact is due to the DS formulation—eqs (2) do not include time derivatives of the stress-tensor components. We will call this scheme FD_DS_SG. The scheme for the x -component is given by eq. (18).

3.5 Scheme solving strong-form velocity-stress equations of motion on the staggered grid—FD_VS_SG

The equations in the VS formulation (4) can be solved by the VS scheme on the staggered grid. In the first and second equations of system (4), we replace the first time derivatives using formula (12),

$$[\partial_t \Phi]^m = \frac{1}{\Delta t} [\Phi^{m+1/2} - \Phi^{m-1/2}], \tag{12}$$

and the first spatial derivatives of the stress-tensor components using formulae (11). Then, we replace all discrete stress-tensor components on the r.h.s. of the obtained scheme by their FD approximations. The approximations are obtained from the third to fifth equations of system (4) using formulae (11) and (12). In the resulting scheme, both discrete particle-velocity and stress-tensor components appear. Unlike the schemes solving DS formulation, the stress-tensor components appear in the resulting scheme because the VS formulation involves time derivatives of the stress-tensor components. We will call the scheme FD_VS_SG.

We could easily include also a VS FD scheme on the partly-staggered grid. We do not do it because the inclusion would not provide any new conclusion compared to that obtained from comparison FD_DS_PSG and FD_DS_SG.

For convenience, the abbreviations and characteristics of all treated numerical schemes are summarized in Table 1.

To make the presentation of the all schemes concise, define auxiliary operators.

$$\begin{aligned} D_{xx} [\Phi(I, L)] &= \Phi(I + 1, L) - 2\Phi(I, L) + \Phi(I - 1, L), \\ D_{zz} [\Phi(I, L)] &= \Phi(I, L + 1) - 2\Phi(I, L) + \Phi(I, L - 1), \\ D_{xz} [\Phi(I, L)] &= \Phi(I + 1, L + 1) - \Phi(I + 1, L - 1) \\ &\quad - \Phi(I - 1, L + 1) + \Phi(I - 1, L - 1), \\ d_x [\Phi(I, L)] &= \Phi(I + 1/2, L) - \Phi(I - 1/2, L), \\ d_z [\Phi(I, L)] &= \Phi(I, L + 1/2) - \Phi(I, L - 1/2), \\ d_{xz} [\Phi(I, L)] &= \Phi(I + 1/2, L + 1/2) - \Phi(I + 1/2, L - 1/2) \\ &\quad - \Phi(I - 1/2, L + 1/2) + \Phi(I - 1/2, L - 1/2). \end{aligned} \tag{13}$$

We define the parameter

$$\gamma = \frac{\Delta t}{h} \beta. \tag{14}$$

Then, the schemes can be written in the concise and unified forms.

FD_D_CG, FE_L

$$\begin{aligned} U_x^{m+1}(I, L) &= 2U_x^m(I, L) - U_x^{m-1}(I, L) \\ &\quad + \gamma^2 \left\{ r^2 D_{xx} [U_x^m(I, L)] + D_{zz} [U_x^m(I, L)] + (r^2 - 1) \frac{1}{4} D_{xz} [U_z^m(I, L)] \right\} \end{aligned} \tag{15}$$

FE_G

$$\begin{aligned} U_x^{m+1}(I, L) &= 2U_x^m(I, L) - U_x^{m-1}(I, L) \\ &\quad + \gamma^2 \left\{ r^2 \left(\frac{1}{6} D_{xx} [U_x^m(I, L - 1)] + \frac{4}{6} D_{xx} [U_x^m(I, L)] + \frac{1}{6} D_{xx} [U_x^m(I, L + 1)] \right) \right. \\ &\quad + \frac{1}{6} D_{zz} [U_x^m(I - 1, L)] + \frac{4}{6} D_{zz} [U_x^m(I, L)] + \frac{1}{6} D_{zz} [U_x^m(I + 1, L)] \\ &\quad \left. + (r^2 - 1) \frac{1}{4} D_{xz} [U_z^m(I, L)] \right\}. \end{aligned} \tag{16}$$

Table 1. Abbreviations and characteristics of the investigated numerical schemes.

	Method	Equation form	Equation formulation	Grid	Integration
FD_D_CG	finite-difference	strong	displacement	conventional	n.a.
FE_L	finite-element	weak	displacement	conventional	Lobatto four-point
FE_G	finite-element	weak	displacement	conventional	Gauss four-point
FE_G1	finite-element	weak	displacement	conventional	Gauss one-point
FD_DS_PSG	finite-difference	strong	displacement-stress	partly-staggered	n.a.
FD_DS_SG	finite-difference	strong	displacement-stress	staggered	n.a.
FD_VS_SG	finite-difference	strong	velocity-stress	staggered	n.a.

FE_G1 , FD_DS_PSG

$$\begin{aligned}
 U_x^{m+1}(I, L) = & 2U_x^m(I, L) - U_x^{m-1}(I, L) \\
 & + \gamma^2 \left\{ r^2 \left(\frac{1}{4} D_{xx} [U_x^m(I, L-1)] + \frac{2}{4} D_{xx} [U_x^m(I, L)] + \frac{1}{4} D_{xx} [U_x^m(I, L+1)] \right) \right. \\
 & + \frac{1}{4} D_{zz} [U_x^m(I-1, L)] + \frac{2}{4} D_{zz} [U_x^m(I, L)] + \frac{1}{4} D_{zz} [U_x^m(I+1, L)] \\
 & \left. + (r^2 - 1) \frac{1}{4} D_{xz} [U_x^m(I, L)] \right\}. \tag{17}
 \end{aligned}$$

FD_DS_SG

$$\begin{aligned}
 U_x^{m+1}(I, L) = & 2U_x^m(I, L) - U_x^{m-1}(I, L) \\
 & + \gamma^2 \{ r^2 D_{xx} [U_x^m(I, L)] + D_{zz} [U_x^m(I, L)] + (r^2 - 1) d_{xz} [U_x^m(I, L)] \}. \tag{18}
 \end{aligned}$$

FD_VS_SG

$$\begin{aligned}
 V_x^{m+1}(I, L) = & V_x^{m-1}(I, L) \\
 & + \frac{\Delta t}{h} \frac{1}{\rho} \{ d_x [S_{xx}^{m-1/2}(I, L)] + d_z [S_{zz}^{m-1/2}(I, L)] \} \\
 & + \gamma^2 \{ r^2 D_{xx} [V_x^m(I, L)] + D_{zz} [V_x^m(I, L)] + (r^2 - 1) d_{xz} [V_x^m(I, L)] \}. \tag{19}
 \end{aligned}$$

Schemes for the z -component of displacement and particle velocity are obtained simply by interchanging x and z in both components and auxiliary operators.

It is interesting to compare the seven numerical schemes. FD_D_CG and FE_L are identical. FE_G is more complicated than FD_D_CG/FE_L but, in fact, it differs from the two schemes only in approximating the second non-mixed spatial derivative. For example, the second non-mixed spatial derivative at gridpoint (I, L) in the x -direction is approximated by a weighted average of the standard centred FD formulae along three grid lines with z -indices, $L - 1$, L and $L + 1$. FD_DS_PSG and FE_G1 are identical and have the same structure as FE_G. The only difference is in the values of the weighting coefficients. The only difference between FD_D_CG/FE_L and FD_DS_SG is in approximating the second mixed derivative. Both schemes use discrete values at corners of a grid square but FD_D_CG's square is $2h \times 2h$, whereas FD_DS_SG's square is $h \times h$. FD_VS_SG differs from FD_DS_SG, apart from the displacements and particle velocities, only in approximating time derivative. All the schemes are illustrated in Fig. 2, which clearly visualizes relatively small differences between them.

4 PLANE S-WAVE PROPAGATION BY THE NUMERICAL SCHEMES

Because modelling P -wave propagation does not pose a problem, we will consider propagation of a harmonic plane S wave in an unbounded homogeneous medium. Let ω be the angular frequency, k_x and k_z components of the wavenumber vector, and δ the angle between the z -axis and direction of propagation of the plane wave. The plane wave is defined by the following relations for the displacement:

$$\begin{aligned}
 u_\zeta(x, z, t; \omega, \delta) &= A_\zeta E^t E^x E^z; \quad \zeta \in \{x, z\} \\
 A_x &= A \cos \delta, \quad A_z = -A \sin \delta \\
 E^t &= \exp[-i\omega t], \quad E^x = \exp[ik_x x], \quad E^z = \exp[ik_z z] \\
 k_x &= k \sin \delta, \quad k_z = k \cos \delta, \quad k = \omega/\beta \tag{20}
 \end{aligned}$$

The plane wave is illustrated in Fig. 3. To obtain numerical schemes specified for the plane-wave propagation we need to substitute expressions for the displacement, particle-velocity and stress-tensor components at some central grid position and neighbouring grid positions in the schemes (15)–(19). They are

$$\begin{aligned}
 u_\zeta(x \pm h, z \pm h, t \pm \Delta t; \omega, \delta) &= A_\zeta E^t E^x E^z \exp[\mp i\omega \Delta t] \exp[\pm i k_x h] \exp[\pm i k_z h], \\
 v_\zeta(x \pm h, z \pm h, t \pm \Delta t; \omega, \delta) &= -i\omega u_\zeta(x \pm h, z \pm h, t \pm \Delta t; \omega, \delta), \\
 \sigma_{\zeta\eta}(x \pm h, z \pm h, t \pm \Delta t; \omega, \delta) &= i A_{\zeta\eta} E^t E^x E^z \exp[\mp i\omega \Delta t] \exp[\pm i k_x h] \exp[\pm i k_z h], \\
 A_{xx} &= (\lambda + 2\mu) k_x A_x + \lambda k_z A_z, \\
 A_{zz} &= (\lambda + 2\mu) k_z A_z + \lambda k_x A_x, \\
 A_{xz} &= \mu k_z A_x + \mu k_x A_z, \quad \zeta, \eta \in \{x, z\}. \tag{21}
 \end{aligned}$$

Let us emphasize that eqs (20) and (21) are exact (analytical) expressions for the displacement, particle velocity and stress of the plane wave in the homogeneous unbounded medium. Consider $x_I = x$, $x_{I\pm 1} = x \pm h$, $z_L = z$, $z_{L\pm 1} = z \pm h$, $t_m = t$, $t_{m-1} = t - \Delta t$ and substitute exact values of the harmonic plane wave (i.e. expressions according to eqs 21) for discrete values of U_x and U_z on the r.h.s. of scheme

Stencils on a uniform square grid			
	stencil for $\frac{\partial}{\partial \zeta}$ → ζ	stencil for $\frac{\partial^2}{\partial \zeta^2}$ → ζ	stencil for $\frac{\partial^2}{\partial x \partial z}$ z ↓ x
<p>FD_VS_SG</p> <p><input type="checkbox"/> velocity</p> <p><input checked="" type="checkbox"/> stress</p>			
<p>FD_DS_SG</p> <p><input type="checkbox"/> displacement</p>	<p>N. A.</p>		
<p>FD_D_CG FE_L</p> <p><input type="checkbox"/> displacement</p>			
<p>FE_G</p> <p><input type="checkbox"/> displacement</p>			
<p>FD_DS_PSG FE_G1</p> <p><input type="checkbox"/> displacement</p>			

Figure 2. Grid stencils for approximating first spatial derivative, non-mixed second spatial derivative and mixed second spatial derivative in the resulting numerical schemes (15)–(19).

FD_D_CG (eq. 15). With

$$2U_x^m(I, L) - U_x^{m-1}(I, L) = A_x E^t E^x E^z (2 - \cos \omega \Delta t - i \sin \omega \Delta t),$$

$$D_{xx} [U_x^m(I, L)] = A_x E^t E^x E^z 2 (\cos k_x h - 1),$$

$$D_{zz} [U_x^m(I, L)] = A_x E^t E^x E^z 2 (\cos k_z h - 1),$$

$$D_{xz} [U_x^m(I, L)] = A_z E^t E^x E^z (-4 \sin k_x h \sin k_z h),$$

(22)

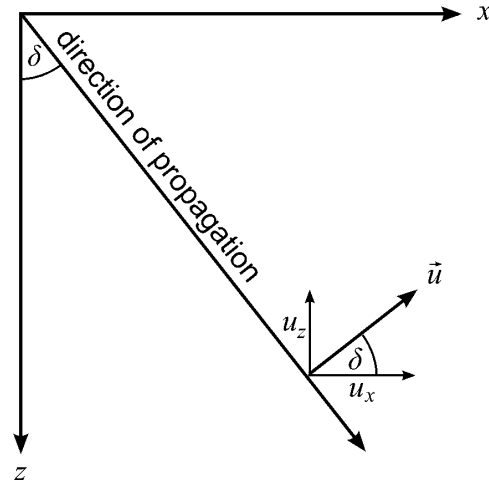


Figure 3. Cartesian coordinate system, angle δ determining a direction of the propagation, displacement vector and displacement components of the plane S wave.

we obtain a scheme for the considered plane wave
FD_D_CG, FE_L

$$\begin{aligned}
 U_x^{m+1}(I, L) = & A_x E^t E^x E^z \left\{ 2 - \cos \omega \Delta t - i \sin \omega \Delta t \right. \\
 & + \gamma^2 \left[r^2 2 (\cos k_x h - 1) + 2 (\cos k_z h - 1) \right. \\
 & \left. \left. - (r^2 - 1) \frac{A_z}{A_x} \sin k_x h \cdot \sin k_z h \right] \right\}. \tag{23}
 \end{aligned}$$

Analogously, we obtain the other schemes
FE_G

$$\begin{aligned}
 U_x^{m+1}(I, L) = & A_x E^t E^x E^z \left\{ 2 - \cos \omega \Delta t - i \sin \omega \Delta t \right. \\
 & + \gamma^2 \left[r^2 2 (\cos k_x h - 1) \frac{2}{6} (\cos k_z h + 2) + 2 (\cos k_z h - 1) \frac{2}{6} (\cos k_x h + 2) \right. \\
 & \left. \left. - (r^2 - 1) \frac{A_z}{A_x} \sin k_x h \cdot \sin k_z h \right] \right\}. \tag{24}
 \end{aligned}$$

FE_G1, FD_DS_PSG

$$\begin{aligned}
 U_x^{m+1}(I, L) = & A_x E^t E^x E^z \left\{ 2 - \cos \omega \Delta t - i \sin \omega \Delta t \right. \\
 & + \gamma^2 \left[r^2 2 (\cos k_x h - 1) \frac{2}{4} (\cos k_z h + 1) + 2 (\cos k_z h - 1) \frac{2}{4} (\cos k_x h + 1) \right. \\
 & \left. \left. - (r^2 - 1) \frac{A_z}{A_x} \sin k_x h \cdot \sin k_z h \right] \right\}. \tag{25}
 \end{aligned}$$

FD_DS_SG

$$\begin{aligned}
 U_x^{m+1}(I, L) = & A_x E^t E^x E^z \left\{ 2 - \cos \omega \Delta t - i \sin \omega \Delta t \right. \\
 & + \gamma^2 \left[r^2 2 (\cos k_x h - 1) + 2 (\cos k_z h - 1) \right. \\
 & \left. \left. - (r^2 - 1) \frac{A_z}{A_x} 4 \sin k_x \frac{h}{2} \cdot \sin k_z \frac{h}{2} \right] \right\}. \tag{26}
 \end{aligned}$$

FD_VS_SG

$$\begin{aligned}
 V_x^{m+1}(I, L) = & -i\omega A_x E^t E^x E^z \left\{ 1 - \left(\cos \omega \frac{\Delta t}{2} - i \sin \omega \frac{\Delta t}{2} \right) \right. \\
 & \times \gamma \left[\left(r^2 \sin \delta + (r^2 - 2) \frac{A_z}{A_x} \cos \delta \right) 2 \sin k_x \frac{h}{2} + \left(\cos \delta + \frac{A_z}{A_x} \sin \delta \right) 2 \sin k_z \frac{h}{2} \right] \\
 & + \gamma^2 \left[r^2 2 (\cos k_x h - 1) + 2 (\cos k_z h - 1) \right. \\
 & \left. \left. - (r^2 - 1) \frac{A_z}{A_x} 4 \sin k_x \frac{h}{2} \cdot \sin k_z \frac{h}{2} \right] \right\}. \tag{27}
 \end{aligned}$$

5 LOCAL ERRORS OF THE NUMERICAL SCHEMES

Without any loss of generality, consider for simplicity $x_l = 0, z_l = 0$ and $t_m = 0$. We can define a local relative error by comparing exact solution (21) for the considered plane wave and numerical solutions—both evaluated at $x_l = 0, z_l = 0$ and $t_{m+1} = \Delta t$. The numerical solutions are obtained from eqs (23)–(27) and corresponding equations for the z -components of the displacement and particle velocity. We recall that eqs (23)–(27) were obtained from numerical schemes (15)–(19) by substituting exact values (exact expressions for the plane wave) for discrete values $U_x, U_z, V_x, V_z, S_{xx}, S_{zz}, S_{xz}$ on the r.h.s. of schemes (15)–(19). A local relative error in amplitude of displacement, ε_a^U , can be defined by

$$\varepsilon_a^U = \frac{1}{(\Delta t)^2} \frac{[(ReU_x)^2 + (ReU_z)^2]^{1/2} - [(Reu_x)^2 + (Reu_z)^2]^{1/2}}{[(Reu_x)^2 + (Reu_z)^2]^{1/2}}, \tag{28}$$

where U_x, U_z, u_x, u_z are evaluated at $x_l = 0, z_l = 0, t_{m+1} = \Delta t$. Because different numerical schemes use different time steps Δt , we normalize the error for a unit time. The use of square of Δt corresponds to the second-order approximation to the time derivative in the equation of motion. The normalization allows a direct comparison of errors of different schemes. It is easy to see that

$$\varepsilon_a^U = \frac{1}{(\Delta t)^2} \left\{ \frac{[(ReU_x)^2 + (ReU_z)^2]^{1/2}}{A \cos \omega \Delta t} - 1 \right\}. \tag{29}$$

Because the exact solution for the particle velocity is

$$v_x(0, 0, \Delta t; \omega, \delta) = -i\omega A \cos \delta \exp[-i\omega \Delta t], \tag{30}$$

$$v_z(0, 0, \Delta t; \omega, \delta) = -i\omega A \sin \delta \exp[-i\omega \Delta t],$$

the error for FD_VS_SG is defined using the imaginary parts of the exact and numerical solutions. Then

$$\varepsilon_a^V = \frac{1}{(\Delta t)^2} \left\{ \frac{[(ImV_x)^2 + (ImV_z)^2]^{1/2}}{\omega A \cos \omega \Delta t} - 1 \right\}. \tag{31}$$

The errors in the direction of the displacement and particle-velocity vectors (i.e. in polarization) can be defined as

$$\varepsilon_\delta^U = \frac{1}{(\Delta t)^2} \frac{\delta^{\text{grid}} - \delta}{\pi}; \quad \delta^{\text{grid}} = \arccos \frac{ReU_x}{[(ReU_x)^2 + (ReU_z)^2]^{1/2}}, \tag{32}$$

and

$$\varepsilon_\delta^V = \frac{1}{(\Delta t)^2} \frac{\delta^{\text{grid}} - \delta}{\pi}; \quad \delta^{\text{grid}} = \arccos \frac{ImV_x}{[(ImV_x)^2 + (ImV_z)^2]^{1/2}}. \tag{33}$$

For brevity, we will call this error ‘an error in angle’. Considering grid spacing h and wavelength λ , we can define a spatial sampling ratio s ,

$$s = h/\lambda. \tag{34}$$

Then

$$k = \omega/\beta = 2\pi s/h, \tag{35}$$

$$k_x h = 2\pi s \sin \delta, \quad k_z h = 2\pi s \cos \delta, \tag{36}$$

$$\omega = 2\pi s\beta/h. \tag{37}$$

A stability condition for any of the considered numerical schemes can be written in the form

$$\Delta t \leq \Psi(h, \alpha, \beta) \tag{38}$$

where Ψ is a function of the grid spacing, and P -wave and S -wave speeds. If we define a stability ratio p ,

$$p = \Delta t/\Psi, \tag{39}$$

Table 2. Time steps and two other quantities appearing in the schemes for the harmonic plane *S* wave, eqs (23)–(27), and local errors (29) and (31)–(33).

	$\omega \Delta t$	$\gamma = (\Delta t/h)\beta$	Δt	
FD_D_CG, FE_L	$2\pi p s \frac{1}{(1+r^2)^{1/2}}$	$\frac{p}{(1+r^2)^{1/2}}$	$P \frac{1}{(1+r^2)^{1/2}} \frac{h}{\beta}$	$P \frac{s}{(1+r^2)^{1/2}} \frac{\lambda}{\beta}$
FD_DS_PSG, FE_G, FE_G1	$2\pi p s \frac{1}{r}$	$\frac{p}{r}$	$P \frac{1}{r} \frac{h}{\beta}$	$P \frac{s}{r} \frac{\lambda}{\beta}$
FD_DS_SG, FD_VS_SG	$\sqrt{2} \pi p s \frac{1}{r}$	$\frac{1}{\sqrt{2}} \frac{p}{r}$	$P \frac{1}{r\sqrt{2}} \frac{h}{\beta}$	$P \frac{s}{r\sqrt{2}} \frac{\lambda}{\beta}$

it is

$$p \leq 1 \tag{40}$$

and the time step can be expressed as

$$\Delta t = p \Psi(h, \alpha, \beta). \tag{41}$$

Quantities $\omega\Delta t$, γ and Δt entering schemes (23)–(27) and consequently also local errors (29) and (31)–(33) are summarized in Table 2.

Consider definitions of the local errors (29), (31)–(33), numerical schemes (23)–(27), relations (36) and quantities in Table 2. We can see that if the definitions of the errors did not include factor $1/(\Delta t)^2$, that is, if the errors were not normalized for the unit time, the local errors would be functions of the spatial sampling ratio s , stability ratio p , P -wave to S -wave speed ratio r and angle δ determining direction of propagation. This would be exactly as one would expect from the very beginning. Because, however, definitions of the local errors are normalized for unit time (for the reason explained before), they do include factor $1/(\Delta t)^2$. Table 2 shows two alternative expressions for the time step Δt . The one in the left-hand column explicitly depends on h/β , and the one in the right-hand column on λ/β . Correspondingly, we can distinguish two possibilities.

In the first possibility, medium (represented by β) and the grid (represented by h) are fixed. The ratio h/β is constant and the same for all schemes. We can omit this ratio and calculate a modified local error as

$$\varepsilon' = \left(\frac{h}{\beta}\right)^2 \varepsilon, \tag{42}$$

where ε stands for any of the errors (29), (31)–(33). Error ε' is a function of the spatial sampling ratio s , stability ratio p , speed ratio r and angle δ . For fixed values of p , r and δ , and varying s , ε' quantifies local error as a function of S -wave wavelength (or frequency) for the fixed medium and grid.

In the second possibility, medium and wavelength λ are fixed. The ratio λ/β is constant and the same for all schemes. We can omit this ratio and calculate a modified local error as

$$\varepsilon'' = \left(\frac{\lambda}{\beta}\right)^2 \varepsilon, \tag{43}$$

where ε stands for any of the errors (29), (31)–(33). Error ε'' is a function of the spatial sampling ratio s , stability ratio p , speed ratio r and angle δ . For fixed values of p , r and δ , and varying s and ε'' quantifies local error as a function of the grid spacing h for the fixed medium and S -wave wavelength (or frequency).

Error $\varepsilon'(s)$ quantifies local error, as it can be ‘seen’ in one simulation (one medium, one grid). Error $\varepsilon''(s)$ quantifies local error for a fixed wavelength as a function of grid spacing h ($s = h/\lambda$, $\lambda = \text{const}$) and is, thus, more suitable for finding value of s for which the local error should not be larger than a reasonable (desired) value. It follows from eqs (42) and (43) that

$$\varepsilon'' = \left(\frac{1}{s}\right)^2 \varepsilon'. \tag{44}$$

6 NUMERICAL RESULTS

Figs 4 and 5 show local error ε' of the investigated numerical schemes as a function of angle δ determining direction of propagation of the plane S wave. The error was calculated for one value of the stability ratio, $p = 0.9$, three values of the spatial sampling ratio, $s \in \{1/12, 1/15, 1/18\}$ and three values of the P -wave to S -wave speed ratio, $r \in \{1.42, 5, 10\}$. $p = 0.9$ was chosen as a reasonable value close to the maximum possible size of the time step. Speed ratio $r = 1.42$ is the minimum possible value of the P -wave to S -wave speed ratio, $r = 5$ is a common value in surface sediments, mainly under the water level and $r = 10$ is not the maximum possible value in unconsolidated surface water-saturated sediments. In other words, $r \geq 5$ often have to be accounted for in the numerical modelling of seismic motion in sedimentary basins and valleys.

Fig. 4 shows local error ε' in amplitude. As expected, for given r and δ , the error of each numerical scheme monotonously decreases with the decreasing spatial sampling ratio s . FD_DS_SG and FD_VS_SG have their maximum errors in the directions of the coordinate axes ($\delta = 0^\circ$) and minimum errors in the direction of the plane diagonal ($\delta = 45^\circ$) for all values of the speed ratio r . It is just opposite with FD_DS_PSG/FE_G1. The behaviour of FD_D_CG/FE_L and FE_G with respect to the direction of propagation is a little bit more

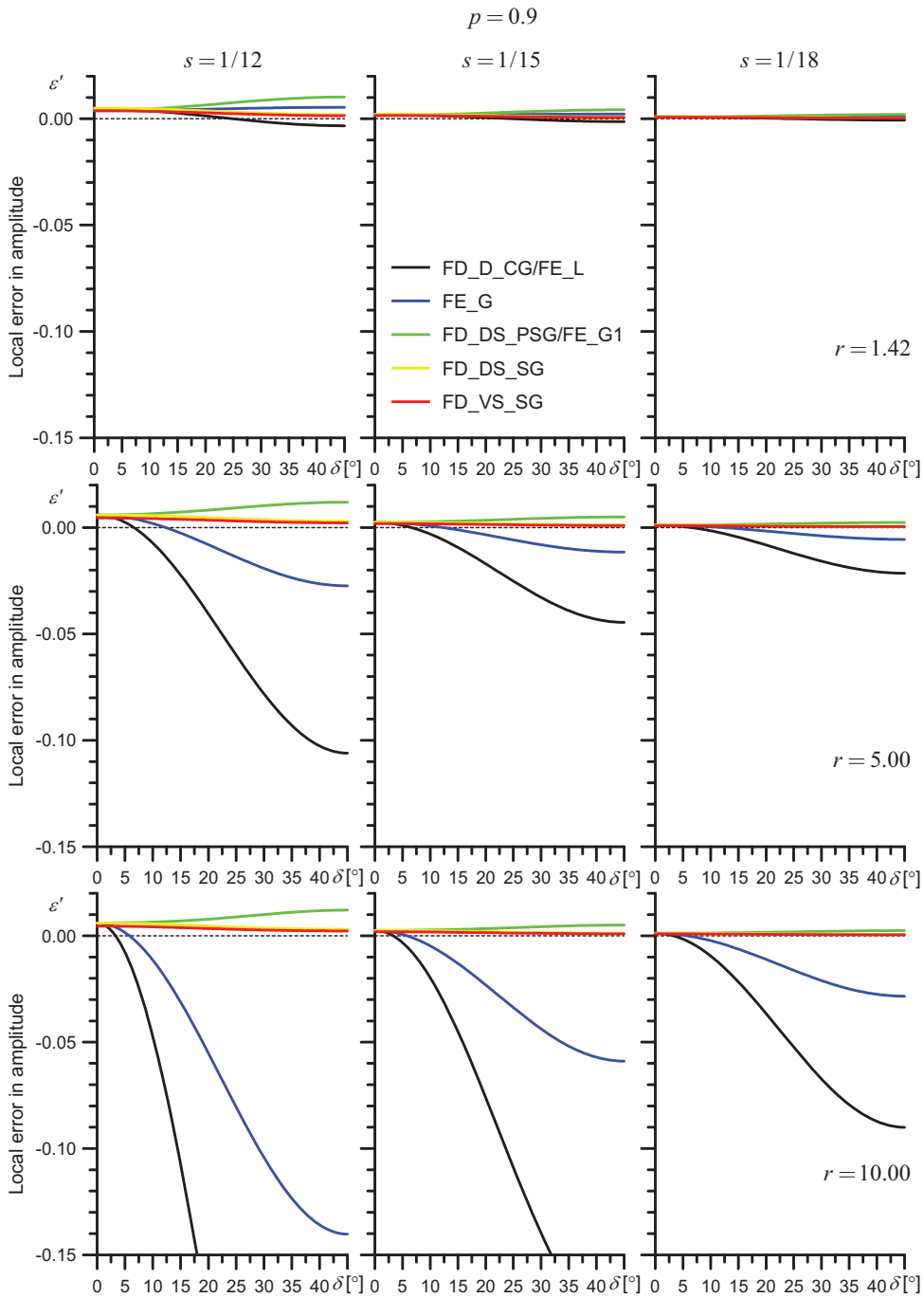


Figure 4. Local error ε' in amplitude as a function of angle δ (in degrees) determining direction of propagation; $\delta = 0^\circ$ corresponds to the z -axis, $\delta = 45^\circ$ corresponds to the xz -diagonal (plane diagonal).

complicated and changes with the speed ratio r . The most important feature of Fig. 4 relates, however, to a very different dependence of the errors of different schemes on the P -wave to S -wave speed ratio r . The errors of all schemes in the directions of the coordinate axes are comparable and not large (in a relative sense). For given δ and s , errors of FD_DS_PSG/FE_G1, FD_DS_SG and FD_VS_SG are practically insensitive to variation in r , whereas errors of FD_D_CG/FE_L and FE_G are sensitive to variation in r . Except for a small range of directions about the coordinate axes (this range narrows with increasing r), the errors of FD_D_CG/FE_L and FE_G attain significantly larger values

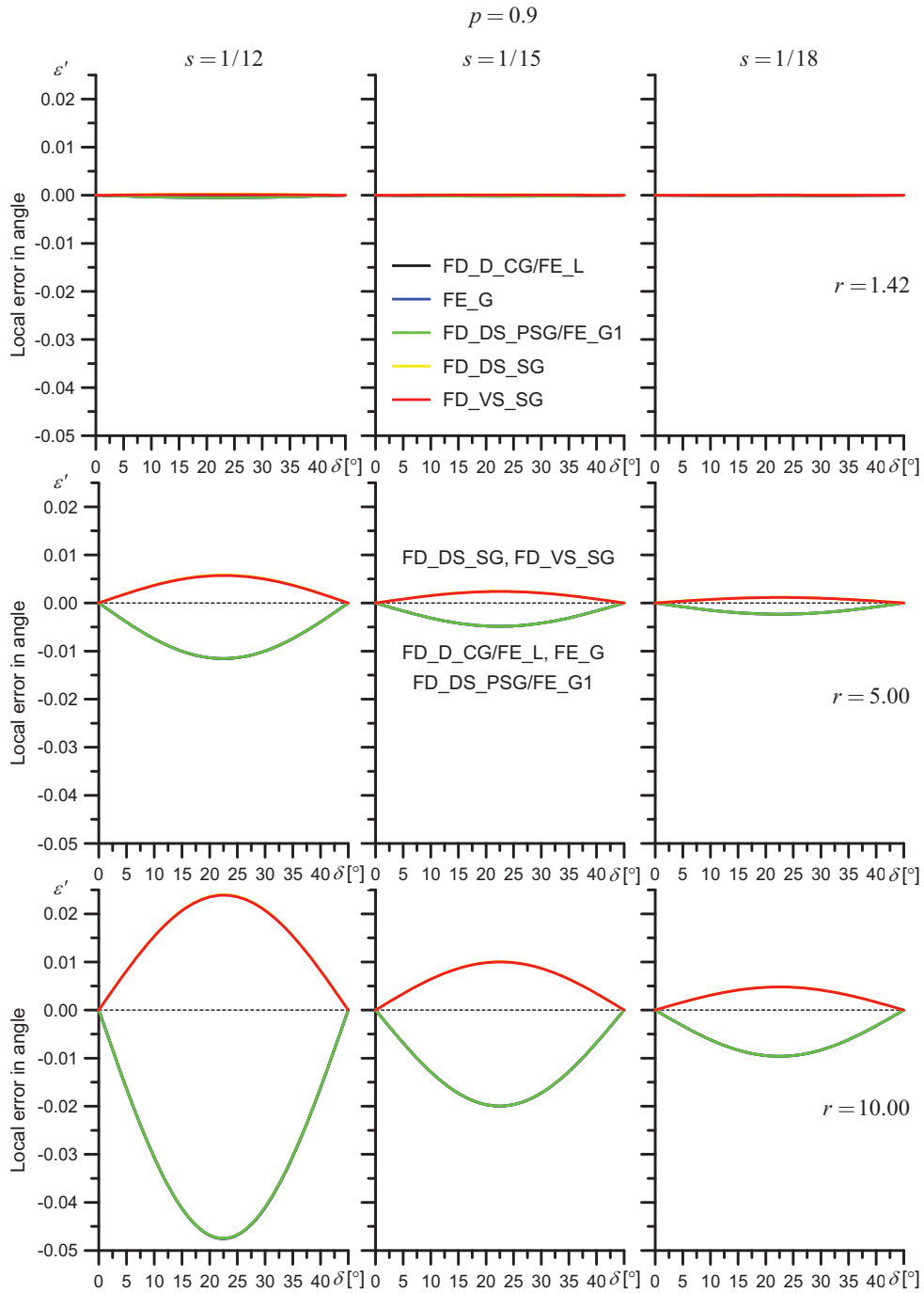


Figure 5. Local error ε' in angle as a function of angle δ (in degrees) determining direction of propagation; $\delta = 0^\circ$ corresponds to the z -axis, $\delta = 45^\circ$ corresponds to the xz -diagonal (plane diagonal).

compared to errors of other schemes for $r = 5$ and $r = 10$. For given δ and s , error of FD_D_CG/FE_L is considerably larger than the error of FE_G.

Clearly, Fig. 4 illustrates important properties of the investigated numerical schemes with respect to the P -wave to S -wave speed ratio r : In general, errors of FD_DS_SG and FD_VS_SG are very close and least sensitive to variation in r and direction of propagation δ , and they are (in comparison to other schemes) small. FD_D_CG/FE_L and FE_G have significantly large errors (in comparison to other schemes) for larger r for directions other than directions of the coordinate axes (the largest errors being in the direction of plane diagonal).

Fig. 5 shows local error ε' in angle (polarization). As expected, for given r and δ , the error of each numerical scheme monotonously decreases with the decreasing spatial sampling ratio s . As also expected, the maximum absolute value of error of each scheme is for $\delta = (45/2)^\circ$. For given δ and s , the absolute value of error of each scheme increases with the increasing speed ratio r . The schemes clearly split into two groups. FD_DS_SG and FD_VS_SG have very close positive errors, whereas FD_D_CG/FE_L, FE_G and FD_DS_PSG/FE_G1 have very close negative errors and their absolute values are larger than absolute values of errors of FD_DS_SG and FD_VS_SG. Overall, the errors in angle of different schemes do not differ as dramatically as the errors in amplitude do for larger values of the speed ratio r . It is interesting that for given δ and s the ratio between absolute values of the errors of any two schemes is independent of the speed ratio r .

Given the dramatic differences between errors in amplitude, it is interesting to illustrate equivalent spatial sampling ratios (i.e. such spatial sampling ratios for which the errors of schemes are equal/comparable). Fig. 6, the left-hand column, shows errors in amplitude of FD_VS_SG and FE_G. For reasons explained in the previous section, it is reasonable to consider error ε'' . Spatial sampling ratio $s = 1/30$ (i.e. 30 grid spacings per wavelength) has to be used with FE_G if the maximum absolute value of error should not be larger than the maximum absolute value of error of FD_VS_SG with $s = 1/12$ for $r = 5$. For $r = 10$ FE_G needs $s = 1/68$ to become comparable with FD_VS_SG with $s = 1/12$. As it is clear from Fig. 4, FD_D_CG/FE_L would need even a considerably smaller spatial sampling ratio.

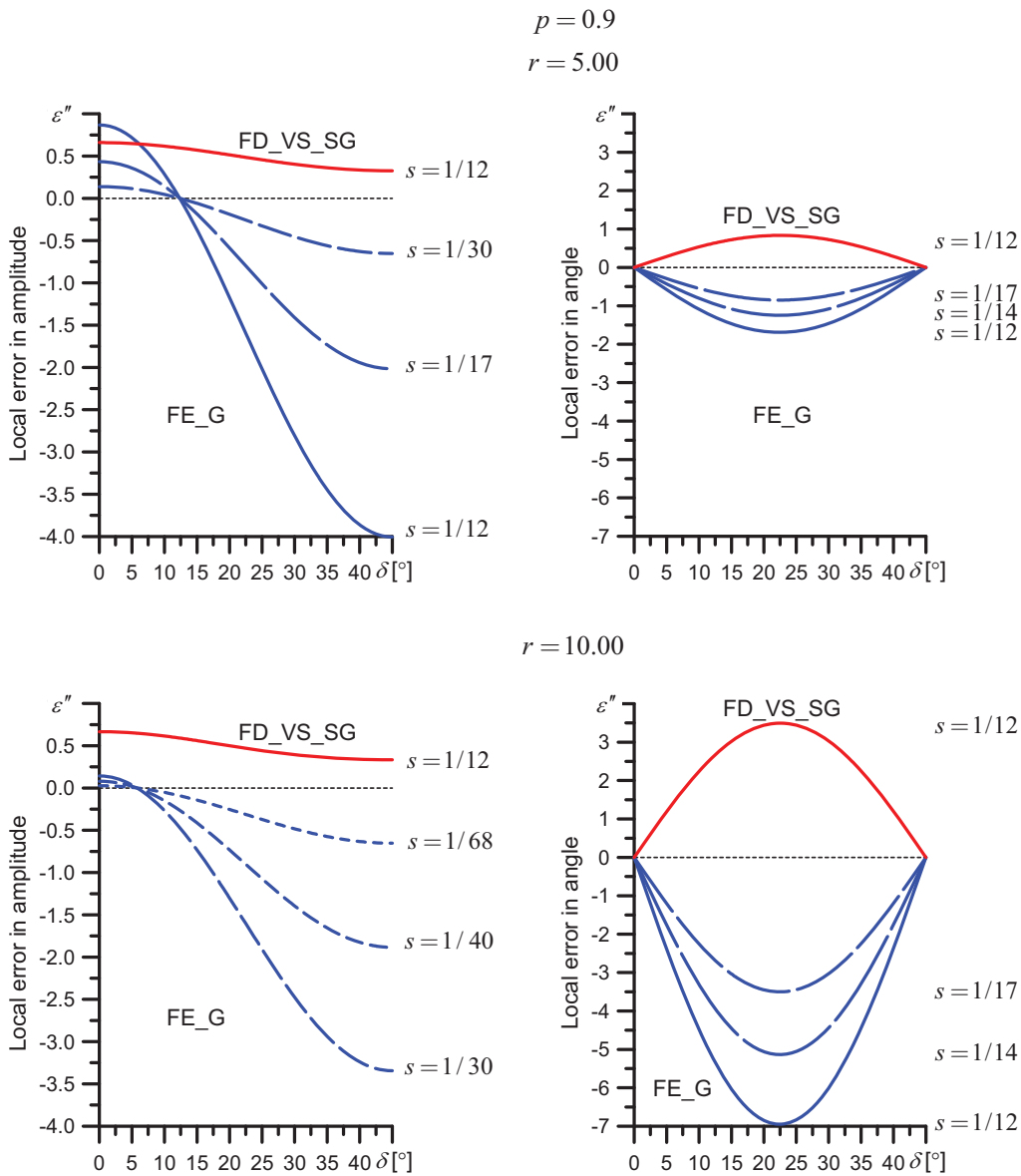


Figure 6. Local error ε'' in amplitude (left-hand column) and angle (right-hand column) as a function of angle δ (in degrees) determining direction of propagation; $\delta = 0^\circ$ corresponds to the z -axis, $\delta = 45^\circ$ corresponds to the xz -diagonal (plane diagonal).

Fig. 6, the right-hand column, shows similar comparisons for errors in angle. As expected, given results in Fig. 5, the equivalent spatial sampling ratios for FE_G, that is, approximately $s = 1/17$, do not differ from $s = 1/12$ for FD_VS_SG as dramatically as in the case of the error in amplitude.

7 DISCUSSION

Having compared errors of the numerical schemes with respect to variation in the P -wave to S -wave speed ratio r (and thus in Poisson's ratio), we can recall schemes (15)–(19) and Fig. 2. Fig. 2 illustrates the schemes in their final resulting (or effective) forms. The figure shows grid stencils for approximating spatial derivatives—the first one, the second non-mixed one and the second mixed one.

FD_DS_SG (18) and FD_VS_SG (19) approximate second spatial derivatives of the displacement and particle velocity in the same way. They differ in approximating time derivatives. FD_DS_SG approximates second time derivative of displacement components, whereas FD_VS_SG approximates first time derivatives of the particle-velocity and stress-tensor components. The very close values of errors suggest that in this case the approximations to time derivatives have only a very small effect on the accuracy of the schemes. The approximations to second spatial derivatives are decisive for small errors and their small sensitivity to variation in r compared to other schemes.

Given the very close errors of FD_DS_SG and FD_VS_SG, let us focus on the comparison between FD_DS_SG (18) and FD_D_CG (15) as representatives of significantly different behaviours with varying r . As already noted, schemes (18) and (15) differ only in the way of approximating the second mixed spatial derivative: FD_D_CG uses discrete values of displacements at corners of square $2h \times 2h$, whereas FD_DS_SG uses discrete values of displacements at corners of square $h \times h$. What does this dissimilarity mean? Perhaps it is more reasonable to view this dissimilarity as a consequence of something at a more elementary level. In deriving FD_DS_SG, all the first spatial derivatives are approximated in the same way—using formulae (11). This is not so with FD_D_CG. In deriving the approximation to the second non-mixed spatial derivative, the central-difference formula over one grid spacing (as in eq. 11) is applied to the first spatial derivatives. However, in deriving the approximation to the second mixed spatial derivative, the central-difference formula over two grid spacings is applied to the first spatial derivatives. In this sense, we can say that the approximating of derivatives in FD_DS_SG is ‘homogeneous’, whereas it is not in FD_D_CG. This difference between the two schemes is reflected in the structures of the truncation errors.

$$\begin{aligned} \text{TrunError}\{\text{FD.D.CG}\} &= -\frac{1}{12}(\Delta t)^2 u_{x,tttt} + O[(\Delta t)^4] \\ &+ h^2 \left\{ \frac{1}{12}\alpha^2 u_{x,xxxx} + \frac{1}{12}\beta^2 u_{x,zzzz} + \frac{1}{3}(\alpha^2 - \beta^2) \left(\frac{1}{2}u_{z,xxxz} + \frac{1}{2}u_{z,xzzz} \right) \right\} + O[h^4]. \end{aligned} \quad (45)$$

$$\begin{aligned} \text{TrunError}\{\text{FD.DS.SG}\} &= -\frac{1}{12}(\Delta t)^2 u_{x,tttt} + O[(\Delta t)^4] \\ &+ h^2 \left\{ \frac{1}{12}\alpha^2 u_{x,xxxx} + \frac{1}{12}\beta^2 u_{x,zzzz} + \frac{1}{12}(\alpha^2 - \beta^2) \left(\frac{1}{2}u_{z,xxxz} + \frac{1}{2}u_{z,xzzz} \right) \right\} + O[h^4]. \end{aligned} \quad (46)$$

Coefficients at $u_{x,xxxx}$, $u_{x,zzzz}$ and $(\frac{1}{2}u_{z,xxxz} + \frac{1}{2}u_{z,xzzz})$ are the same in FD_DS_SG: $\frac{1}{12}$. In FD_D_CG they are $\frac{1}{12}$ at $u_{x,xxxx}$ and $u_{x,zzzz}$ but $\frac{1}{3}$ at $(\frac{1}{2}u_{z,xxxz} + \frac{1}{2}u_{z,xzzz})$.

Apparently we cannot change the approximation to the second mixed derivative on the conventional grid. However, we can speculate with the approximation to the second non-mixed derivative. To ‘homogenize’ the approximations, let us apply the central-difference formula over two grid spacings to approximate the first spatial derivatives in deriving an approximation to the second non-mixed derivatives. We then get

$$\begin{aligned} [\partial_{xx}\Phi](I, L) &= \frac{1}{4h^2} [\Phi(I+2, L) - 2\Phi(I, L) + \Phi(I-2, L)], \\ [\partial_{zz}\Phi](I, L) &= \frac{1}{4h^2} [\Phi(I, L+2) - 2\Phi(I, L) + \Phi(I, L-2)], \\ [\partial_{xz}\Phi](I, L) &= \frac{1}{4h^2} [\Phi(I+1, L+1) - \Phi(I+1, L-1) \\ &\quad - \Phi(I-1, L+1) + \Phi(I-1, L-1)], \end{aligned} \quad (47)$$

instead of approximations (9). Clearly, the approximations to the second non-mixed derivatives are less accurate than those in (9). However, the only interesting question now is how this ‘homogenized’ scheme behaves with the varying speed ratio r . The numerical calculation of the errors confirms that the scheme is practically insensitive to the varying r .

Does it mean that we have found a conventional-grid scheme that is not sensitive to the varying r ? No, it does not. If we look closely at the scheme, it is nothing else than the displacement-stress scheme on the staggered grid with a grid spacing equal to $2h$.

Thus, the analysis suggests that the ‘heterogeneity’ (in the described sense) in approximating spatial derivatives is responsible for the poor behaviour of FD_D_CG with an increasing value of the speed ratio r .

8 CONCLUSIONS

We analysed seven numerical schemes for their behaviour with a varying P -wave to S -wave speed ratio (i.e. indirectly, with a varying Poisson's ratio).

FD schemes are as follows:

- (1) displacement on a conventional grid (FD_D_CG),
- (2) displacement-stress on a partly-staggered grid (FD_DS_PSG),
- (3) displacement-stress on a staggered grid (FD_DS_SG) and
- (4) velocity-stress on a staggered grid (FD_VS_SG).

FE schemes are as follows:

- (1) with Lobatto four-point integration (FE_L),
- (2) with Gauss four-point integration (FE_G) and
- (3) with Gauss one-point integration (FE_G1).

To identify very basic inherent aspects of the schemes responsible for their behaviour with varying r , and to compare different types of schemes at the most fundamental level, we analysed schemes that are basic in terms of the order of approximation second-order, and dimensionality, 2-D, for an elastic homogeneous isotropic medium and a uniform grid. We presented all the schemes in a unified form.

Because the spatial sampling has to account for the S wave, we considered propagation of plane S wave and derived specific schemes.

We defined (full) local errors of the schemes in amplitude and polarization in one time step. Because different schemes use different time steps (following the appropriate stability conditions), we normalized the errors for a unit time. The normalization enabled us to directly compare errors of the investigated schemes.

Accuracy of the FD scheme on the conventional grid, FD_D_CG, strongly depends on r . A computationally efficient application to sedimentary basins with a large speed ratio is practically impossible.

Errors of the FD schemes on the staggered grid, FD_DS_SG and FD_VS_SG, are very close and small (in comparison to other schemes). The difference in errors is just due to different time integrations in the schemes. The errors are practically insensitive to variation in r .

Considering the negligible difference between errors of FD_DS_SG and FD_VS_SG, schemes FD_D_CG (displacement scheme on the conventional grid, eq. 15) and FD_DS_SG (displacement-stress on the staggered grid eq. 18) can be considered representative of the significantly different behaviours with varying r . The only apparent difference between the two schemes is in the way of approximating the second mixed spatial derivative. Where does it come from? In deriving FD_DS_SG, only one and the same approximation formula is applied to all the first spatial derivatives. It is not so in FD_D_CG: one approximation formula is applied to the first spatial derivative in deriving the approximation to the second non-mixed derivative, whereas a different approximation formula is applied to the first spatial derivative in deriving the approximation to the second mixed derivative. The 'heterogeneity' in approximating the first spatial derivatives seems to be the key factor causing the sensitivity of the scheme to varying r and the inaccuracy of the scheme for large r .

Our results indicate that not only displacement FD schemes on the conventional grid but also displacement FE schemes on the conventional grid are inaccurate in media with a large P -wave to S -wave speed ratio if commonly used spatial sampling is applied. FE_G1, identical with FD_DS_PSG, is an exception but (as it is well known) the scheme suffers from the presence of the hour-glass modes that have to be artificially suppressed.

The dimensionality of the problem hardly plays a role. In other words, we think that these results are also valid for the second-order 3-D FD and FE displacement schemes. Thus the results indicate that the application of these schemes to real sedimentary basins in general requires sufficiently fine spatial grids—considerably finer than usually applied.

Clearly, this study has to be complemented by a one focusing on the higher-order 3-D schemes to see how the higher order approximations in the investigated types of schemes affect the behaviour with respect to the varying P -wave to S -wave speed ratio. Based on the presented analysis and also our preliminary investigations, we envisage that the higher order itself will not help.

ACKNOWLEDGMENTS

This work was supported in part by the Slovak Research and Development Agency under the contract No. APVV-0435-07 (project OPTIMODE) and VEGA Project 1/4032/07. We gratefully acknowledge the funding by the European Union through the Initial Training Network QUEST (grant agreement No. 238007), a Marie Curie Action under the People Programme. We greatly appreciate Martin Käser's careful and detailed review. Comments of an anonymous reviewer also helped to improve the article. We also thank Jean Virieux, Emmanuel Chaljub, Brad Aagaard, Shuo Ma and Ralph Archuleta for useful discussions.

REFERENCES

- Alford, R.M., Kelly, K.R. & Boore, D.M., 1974. Accuracy of finite-difference modeling of the acoustic wave equation, *Geophysics*, **39**, 834–842.
- Alterman, Z. & Karal, F.C., 1968. Propagation of elastic waves in layered media by finite-difference methods, *Bull. seism. Soc. Am.*, **58**, 367–398.
- Alterman, Z. & Loewenthal, D., 1970. Seismic waves in a quarter and three-quarter plane, *Geophys. J. R. astr. Soc.*, **20**, 101–126.

- Alterman, Z. & Rotenberg, A., 1969. Seismic waves in a quarter plane, *Bull. seism. Soc. Am.*, **59**, 347–368.
- Andrews, D.J., 1973. A numerical study of tectonic stress release by underground explosions, *Bull. seism. Soc. Am.*, **63**, 1375–1391.
- Bamberger, A., Chavent, G. & Lailly, P., 1980. Etude de schémas numériques pour les équations de l'élastodynamique linéaire, Technical Report 41, INRIA, 1980.
- Bielak J., Loukakis, K., Hisada, Y. & Yoshimura, Ch., 2003. Domain reduction method for three-dimensional earthquake modeling in localized regions. Part I: theory, *Bull. seism. Soc. Am.*, **93**, 817–824.
- Boore, D.M., 1970. Love waves in non-uniform waveguides: finite difference calculations, *J. geophys. Res.*, **75**, 1512–1527.
- Boore, D.M., 1972. Finite-difference methods for seismic wave propagation in heterogeneous materials, in *Methods in Computational Physics*, pp. 1–37, Vol. 11, ed. Bolt B.A., Academic Press, New York.
- Chaljub, E., Komatitsch, D., Vilotte, J.-P., Capdeville, Y., Valette, B. & Festa G., 2007. Spectral element analysis in seismology, in *Advances in Wave Propagation in Heterogeneous Earth*, pp. 365–419, eds Wu R.-S. & Maupin V., *Advances in Geophysics* Vol. 48, ed. Dmowska R., Elsevier – Academic Press, Oxford.
- Crase, E., Wideman, Ch., Noble, M. & Tarantola, A., 1992. Nonlinear elastic waveform inversion of land seismic reflection data, *J. geophys. Res.*, **97**, 4685–4703.
- Day, S.M., 1977. Finite element analysis of seismic scattering problems, *PhD thesis*, University of California, San Diego.
- Day, S.M., 1982. Three-dimensional simulation of spontaneous rupture: the effect of non-uniform prestress, *Bull. seism. Soc. Am.*, **72**, 1881–1902.
- de la Puente, J., Käser, M., Dumbser, M. & Igel, H., 2007. An arbitrary high order discontinuous Galerkin method for elastic waves on unstructured meshes IV: anisotropy, *Geophys. J. Int.*, **169**, 1210–1228.
- de la Puente, J., Dumbser, M., Käser, M. & Igel, H., 2008. Discontinuous Galerkin methods for wave propagation in poroelastic media, *Geophysics*, **73**, T77–T97.
- Dumbser, M. & Käser, M., 2006. An arbitrary high order discontinuous Galerkin method for elastic waves on unstructured meshes II: the three-dimensional case, *Geophys. J. Int.*, **167**, 319–336.
- Dumbser, M., Käser, M. & Toro, E., 2007. An arbitrary high order discontinuous Galerkin method for elastic waves on unstructured meshes V: local time stepping and p-adaptivity, *Geophys. J. Int.*, **171**, 695–717.
- Geller, R.J. & Takeuchi, N., 1995. A new method for computing highly accurate DSM synthetic seismograms, *Geophys. J. Int.*, **123**, 449–470.
- Geller, R.J. & Takeuchi, N., 1998. Optimally accurate second-order time-domain finite difference scheme for the elastic equation of motion: one-dimensional case, *Geophys. J. Int.*, **135**, 48–62.
- Graves, R.W., 1996. Simulating seismic wave propagation in 3D elastic media using staggered-grid finite differences, *Bull. seism. Soc. Am.*, **86**, 1091–1106.
- Hughes, T.J.R., 2000. *The Finite Element Method Linear Static and Dynamic Finite Element Method Analysis*, Dover Publications Inc., New York.
- Igel, H., Mora, P. & Rioulet, B., 1995. Anisotropic wave propagation through finite-difference grids, *Geophysics*, **60**, 1203–1216.
- Ilan, A., Ungar, A. & Alterman, Z.S., 1975. An improved representation of boundary conditions in finite difference schemes for seismological problems, *Geophys. J. R. astr. Soc.*, **43**, 727–745.
- Käser, M. & Dumbser, M., 2006. An arbitrary high order discontinuous Galerkin method for elastic waves on unstructured meshes I: the two-dimensional isotropic case with external source terms, *Geophys. J. Int.*, **166**, 855–877.
- Käser, M., Dumbser, M., de la Puente, J. & Igel, H., 2007. An arbitrary high order discontinuous Galerkin method for elastic waves on unstructured meshes III: viscoelastic attenuation, *Geophys. J. Int.*, **168**, 224–242.
- Käser, M., Hermann, V. & de la Puente, J., 2008. Quantitative accuracy analysis of the discontinuous Galerkin method for seismic wave propagation, *Geophysical J. Int.*, **173**, 990–999.
- Kelly, K.R., Ward, R.W., Treitel, S. & Alford, R.M., 1976. Synthetic seismograms: a finite-difference approach, *Geophysics*, **41**, 2–27.
- Klimeš, L., 1996. Accuracy of elastic finite differences in smooth media, *Pageoph*, **148**, 39–76.
- Komatitsch, D. & Vilotte, J.-P., 1998. The spectral-element method: an efficient tool to simulate the seismic response of 2D and 3D geological structures, *Bull. seism. Soc. Am.*, **88**, 368–392.
- Komatitsch, D. & Tromp J., 1999. Introduction to the spectral element method for three-dimensional seismic wave propagation, *Geophys. J. Int.*, **139**, 806–822.
- Komatitsch, D., Martin, R., Tromp, J., Taylor, M.A. & Wingate, B.A., 2001. Wave propagation in 2-D elastic media using a spectral element method with triangles and quadrangles, *J. comput. Acoustics*, **9**, 703–718.
- Kristek, J. & Moczo, P., 2006. On the accuracy of the finite-difference schemes: the 1D elastic problem, *Bull. seism. Soc. Am.*, **96**, 2398–2414.
- Levander, A., 1988. Fourth-order finite-difference P-SV seismograms, *Geophysics*, **53**, 1425–1436.
- Luo, Y. & Schuster, G., 1990. Parsimonious staggered grid finite-differencing of the wave equation, *Geophys. Res. Lett.*, **17**, 155–158.
- Lysmer, J., 1970. Lumped mass method for Rayleigh waves, *Bull. seism. Soc. Am.*, **60**, 89–104.
- Lysmer, J. & Drake, L.A., 1971. The propagation of Love waves across non-horizontally layered structures, *Bull. seism. Soc. Am.*, **61**, 1233–1252.
- Lysmer, J. & Drake, L.A., 1972. A finite element method for seismology, in *Methods in Computational Physics*, pp. 181–216, Vol. 11, ed. Bolt B.A., Academic Press, New York.
- Ma, S. & Liu, P., 2006. Modeling of the perfectly matched layer absorbing boundaries and intrinsic attenuation in explicit finite-element methods, *Bull. seism. Soc. Am.*, **96**, 1779–1794.
- Magnier, S.-A., Mora P. & Tarantola, A., 1994. Finite differences on minimal grids, *Geophysics*, **59**, 1435–1443.
- Marfurt, K.J., 1984. Accuracy of finite-difference and finite-element modeling of the scalar and elastic wave equations, *Geophysics*, **49**, 533–549.
- Moczo, P., Kristek, J. & Bystrický, E., 2000a. Stability and grid dispersion of the P-SV 4th-order staggered-grid finite-difference schemes, *Studia Geophys. Geod.*, **44**, 381–402.
- Moczo, P., Kristek, J. & Halada, L., 2000b. 3D 4th-order staggered-grid finite-difference schemes: stability and grid dispersion, *Bull. seism. Soc. Am.*, **90**, 587–603.
- Moczo, P., Kristek, J., Vavryčuk, V., Archuleta, R.J. & Halada, L., 2002. 3D heterogeneous staggered-grid finite-difference modeling of seismic motion with volume harmonic and arithmetic averaging of elastic moduli and densities, *Bull. seism. Soc. Am.*, **92**, 3042–3066.
- Moczo, P., Kristek, J., Galis, M., Pazak, P. & Balazovjech, M., 2007a. The finite-difference and finite-element modeling of seismic wave propagation and earthquake motion, *Acta Phys. Slovaca*, **57**, 177–406.
- Moczo, P., Robertsson, J.O.A. & Eisner, L., 2007b. The finite-difference time-domain method for modeling of seismic wave propagation, in *Advances in Wave Propagation in Heterogeneous Earth*, pp. 421–516, Vol. 48, eds Wu, R.-S., Maupin, V. & Dmowska, R., in the series *Advances in Geophysics*, Elsevier/Academic Press, San Diego.
- Olsen, K.B., Archuleta, R.J. & Matarese, J.R., 1995. Magnitude 7.75 earthquake on the San Andreas fault: three-dimensional ground motion in Los Angeles, *Science*, **270**, 1628–1632.
- Pitarka, A., 1999. 3D elastic finite-difference modeling of seismic motion using staggered grids with nonuniform spacing, *Bull. seism. Soc. Am.*, **89**, 54–68.
- Rodrigues, D. & Mora, P., 1992. Analysis of a finite-difference solution to the three-dimensional elastic wave equation, in the *62nd Ann. Intemat. Mtg., Expl. Geophys.*, Expanded Abstracts, 1247–1249.
- Saenger, E.H. & Bohlen, T., 2004. Finite-difference modeling of viscoelastic and anisotropic wave propagation using the rotated staggered grid, *Geophysics*, **69**, 583–591.
- Saenger, E.H., Gold, N. & Shapiro, S.A., 2000. Modeling the propagation of elastic waves using a modified finite-difference grid, *Wave Motion*, **31**, 77–92.
- Seriani, G. & Priolo, E., 1991. High-order spectral element method for acoustic wave modeling, *Expanded abstracts of the Soc. Expl. Geophys.*, 1561–1564.
- Seriani, G. & Priolo, E., 1994. A spectral element method for acoustic wave simulation in heterogeneous media, *Finite Elem. in Anal. and Des.*, **16**, 337–348.

- Smith, W.D., 1975. The application of finite element analysis to body wave propagation problems, *Geophys. J.*, **42**, 747–768.
- Stephen, R.A., 1983. A comparison of finite difference and reflectivity seismograms for marine models, *Geophys. J. R. astr. Soc.*, **72**, 39–57.
- Takeuchi, N. & Geller, R.J., 2000. Optimally accurate second order time-domain finite difference scheme for computing synthetic seismograms in 2-D and 3-D media, *Phys. Earth planet. Int.*, **119**, 99–131.
- Virieux, J., 1984. SH-wave propagation in heterogeneous media: velocity-stress finite-difference method, *Geophysics*, **49**, 1933–1957.
- Virieux, J., 1986. P-SV wave propagation in heterogeneous media: velocity-stress finite-difference method, *Geophysics*, **51**, 889–901.
- Yoshimura Ch., Bielak, J., Hisada, Y. & Fernández, A., 2003. Domain reduction method for three-dimensional earthquake modeling in localized regions, Part II: verification and applications, *Bull. seism. Soc. Am.*, **93**, 825–840.
- Zhang, J., 1997. Quadrangle-grid velocity-stress finite-difference method for elastic-wave-propagation simulation, *Geophys. J. Int.*, **131**, 127–134.
- Zienkiewicz, O.C. & Taylor, R.L., 1989. *The Finite Element Method*, 4th edn, Vol. 1, McGraw-Hill.

The definitive version is available at www.blackwell-synergy.com.
<http://www3.interscience.wiley.com/cgi-bin/fulltext/123194893/PDFSTART>